

Describing isotropic and anisotropic out-of-plane deformations in thin cubic materials by use of Zernike polynomials

Chih-Hao Chang, Mireille Akilian, and Mark L. Schattenburg

Isotropic and anisotropic out-of-plane deformations induced by thin-film residual stress on thin cubic materials are studied. By transforming the compliance tensor, an analytical expression can be derived for the biaxial stiffness modulus for all directions in any given cubic crystal plane. A modified Stoney's equation, including both isotropic and anisotropic terms, can be formulated to predict the anisotropic out-of-plane deformation. The isotropic and anisotropic deformations are then described using the Zernike polynomials U_{21} and U_{22} , respectively. Experimental results from (100) and (110) silicon wafers confirm the model by quantitatively comparing the changes in Z_{21} and Z_{22} coefficients due to thin-film stress. © 2006 Optical Society of America

OCIS codes: 120.0120, 310.1860.

1. Introduction

Out-of-plane deformation of flat surfaces induced by thin-film residual stress¹ is an important issue in microelectronic devices, microelectromechanical system fabrication, and coating of thin optical elements. For cubic materials, depending on the orientation of the plane under study, the deformation can be either directionally dependent or independent. In this paper we report analysis and characterization of isotropic and anisotropic out-of-plane deformations in (100) and (110) cubic materials using Zernike polynomials.

Significant interest has been placed on (110) orientation silicon wafers for micromachining. When properly processed with anisotropic wet etchants, such as potassium hydroxide or tetramethyl ammonium hydroxide, fabricated structures can result in near atomically smooth vertical walls.² Silicon wafers with off-cut orientation can also produce unique surface profiles, such as blazed reflection gratings for x -ray spectroscopy.^{3,4} The biaxial stiffness modulus for cubic material with such orientation is anisotropic, and

stress from deposited films will lead to anisotropic out-of-plane deformation.

The well-known Stoney's equation,⁵ most commonly used to describe isotropic out-of-plane deformation for thin films on plates, is given by

$$\frac{1}{R} = \frac{6\sigma_o t}{E_{bi} h^2}, \quad (1)$$

where R is the radius of curvature; σ_o is the film stress; E is Young's modulus; ν is the Poisson's ratio of the material; $E_{bi} = E/(1 - \nu)$ is the biaxial stiffness modulus of the plate; and t and h are the thickness of the film and plate, respectively. For a given crystal plane, anisotropic out-of-plane strain arises when E_{bi} is dependent on direction. Brantley⁶ has examined various crystal planes for cubic materials and has shown that E_{bi} is invariant of direction in {100} and {111}, while being anisotropic in {110} crystal planes. A modified Stoney's equation, combined with Zernike polynomials, can be derived to describe the anisotropic out-of-plane deformation in {110} crystal planes for cubic materials.

Using Stoney's equation, curvature measurements along a single lattice direction can experimentally determine the film stress based on its induced curvature.^{7,8} For isotropic deformation, the relationship can be generalized to all directions in the plane. Complications arise when anisotropic deformation is measured, such as epitaxial strain,⁹ and typically only a

The authors are with the Space Nanotechnology Laboratory, Massachusetts Institute of Technology, 70 Vassar Street, Room 37-420, Cambridge, Massachusetts 02139. The e-mail address for C.-H. Chang is chichang@mit.edu.

Received 10 March 2005; revised 6 September 2005; accepted 10 October 2005.

0003-6935/06/030432-06\$15.00/0

© 2006 Optical Society of America

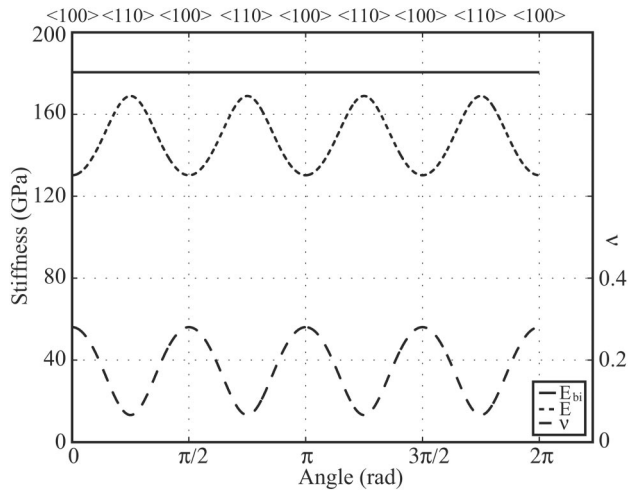


Fig. 1. E_{bi} , E , and ν of silicon as functions of angle from the $\langle 100 \rangle$ direction within the (100) plane.

few principal directions are measured. Using the Zernike polynomial characterization described in this paper, the relationship between film stress and anisotropic curvature can be obtained.

2. E_{bi} for (100) and (110) Planes in Cubic Materials

To calculate E and ν for an arbitrary Miller indices direction $[hkl]$, tensor transformation can be used to transform the fourth-order compliant tensor from the given coordinate system to the $[hkl]$ direction. As previously described by Brantley,⁶ for an arbitrary direction in a cubic material, E is

$$E = \frac{1}{s_{11}} = \frac{1}{s_{11} - 2S(l_1^2 l_2^2 + l_2^2 l_3^2 + l_1^2 l_3^2)}, \quad (2)$$

and ν is

$$\nu_{12} = -\frac{s_{12}'}{s_{11}'} = -\frac{s_{12} + S(l_1^2 m_1^2 + l_2^2 m_2^2 + l_3^2 m_3^2)}{s_{11} - 2S(l_1^2 l_2^2 + l_2^2 l_3^2 + l_1^2 l_3^2)}, \quad (3)$$

where s_{11} , s_{12} , and s_{44} are the three independent compliance constants of the cubic material; and $S = s_{11} - s_{11} - (\frac{1}{2})s_{44}$ and l_i and m_i are the direction cosines for $[hkl]$ and its associated shear direction. Using Eqs. (2) and (3), the effects of the anisotropic stiffness can be predicted in (100) and (110) planes for cubic materials.

For directions in the (100) plane,⁶ E_{bi} is given by

$$E_{bi,(100)} = \frac{1}{s_{11} + s_{12}}. \quad (4)$$

Using the compliant constants of silicon outlined in Mason¹⁰ and Eq. (4), E_{bi} for directions in the (100) plane are plotted as a function of angle from the $\langle 100 \rangle$ direction, as shown in Fig. 1. The plot of E_{bi} is direction invariant, and therefore the out-of-plane deformation for a (100) plane is isotropic. Combining

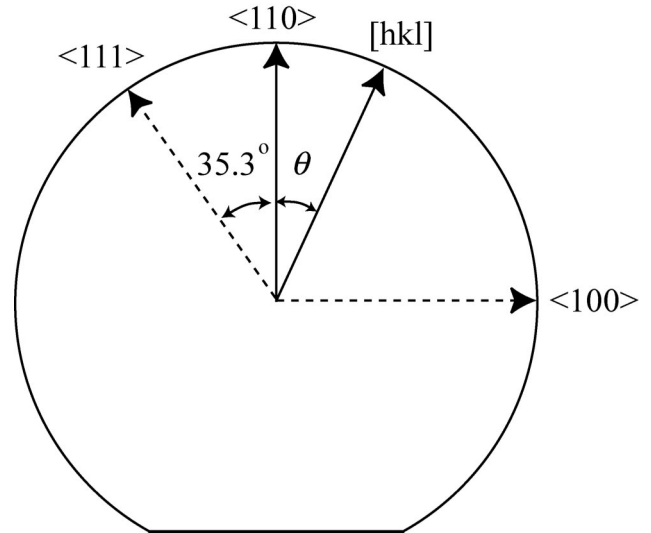


Fig. 2. Reference frame of (110) silicon plane. Some common directions are labeled.

$E_{bi,(100)}$ with Eq. (1), the radius of curvature induced by the film stress can be derived as a function of the compliance constants

$$\frac{1}{R_{(100)}} = \frac{6\sigma_o t}{h^2} (s_{11} + s_{12}). \quad (5)$$

For (110) crystal planes, let the arbitrary direction $[hkl]$ lie on the (110) plane and at an angle θ to the $\langle 110 \rangle$ direction, as shown in Fig. 2. The direction cosines will then be

$$[l_1, l_2, l_3] = \left[\frac{\sqrt{2}}{2} \cos \theta, -\frac{\sqrt{2}}{2} \cos \theta, \sqrt{1 - \cos^2 \theta} \right],$$

$$[m_1, m_2, m_3] = \left[\frac{\sqrt{2}}{2} \sin \theta, -\frac{\sqrt{2}}{2} \sin \theta, \sqrt{1 - \sin^2 \theta} \right]. \quad (6)$$

Combining with Eqs. (2) and (3) yields

$$E_{bi(110)}(\theta) = \frac{1}{s_{11} + s_{12} + S\left(\frac{3}{2} \cos^4 \theta + \frac{3}{2} \cos^2 \theta \sin^2 \theta - 2 \cos^2 \theta\right)}. \quad (7)$$

Substituting trigonometric identities and simplifying, we obtain

$$E_{bi(110)}(\theta) = \frac{1}{s_{11} + s_{12} - \frac{S}{4} (\cos 2\theta + 1)}. \quad (8)$$

Using Eq. (8), the E , ν , and E_{bi} for (110) silicon planes are plotted as functions of direction, as shown in Fig. 3. From the plot, the E_{bi} has maximum and minimum values of 264.6 and 180.6 GPa along the $\langle 110 \rangle$ and

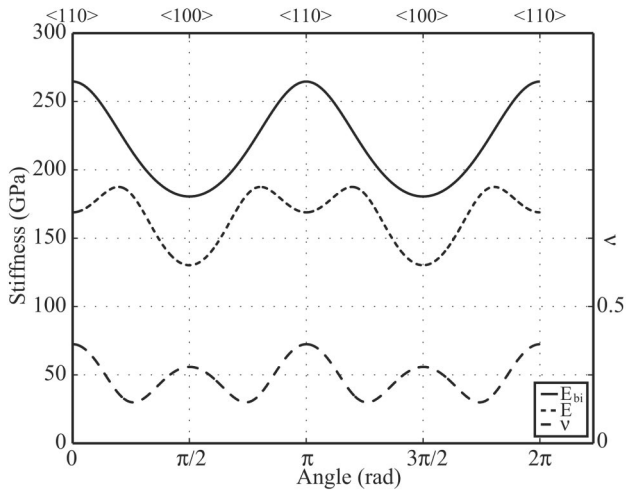


Fig. 3. E_{bi} , E , and ν of silicon as functions of angle from the $\langle 110 \rangle$ direction within the (110) plane.

$\langle 100 \rangle$ directions, respectively. Combining $E_{bi, (110)}$ with Eq. (1) yields a direction-dependent Stoney's equation,

$$\frac{1}{R_{(110)}(\theta)} = \frac{6\sigma_0 t}{h^2} \left(s_{11} + s_{12} - \frac{S}{4} \right) - \frac{3\sigma_0 t}{2h^2} S \cos 2\theta, \quad (9)$$

where the curvature is expressed as a function of isotropic and anisotropic terms. The anisotropic term has angular frequency of $1/\pi$, and its ratio to the isotropic term will be dependent on the material's compliance constants only. Using Eq. (9) the anisotropic out-of-plane deformation on a (110) plane for any given cubic material can be predicted.

3. Zernike Polynomials

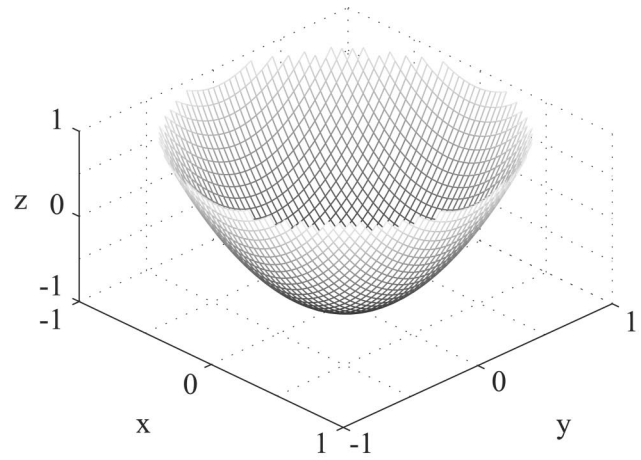
For the case of circular plates, such as wafers used in microfabrication processes, the surface profile can be expressed as a linear combination of mathematical functions known as Zernike polynomials. Zernike polynomials are a set of orthogonal polynomials within a unit circle, commonly used to describe optical wavefront aberrations.¹¹ Because of their orthogonality property, the effect of each polynomial can be studied independently. By examining the Zernike polynomials representing the deformed surface, different modes of distortion can be analyzed to provide a better description of both isotropic and anisotropic out-of-plane deformations.

The Zernike polynomials are defined in polar coordinates as

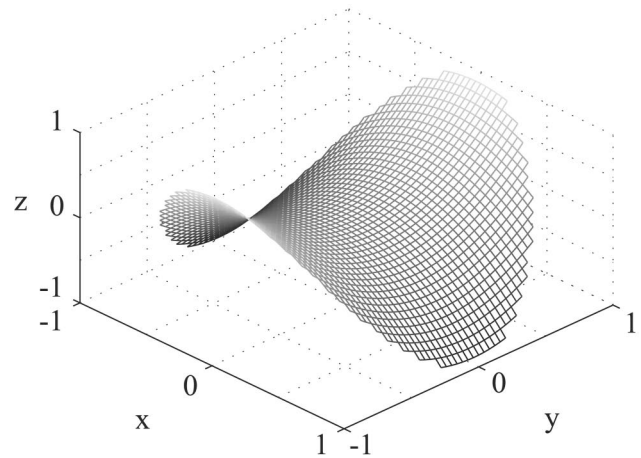
$$\begin{aligned} \text{even } U_n^l(\rho, \theta) &= R_n^l(\rho) \cos(l\theta), \\ \text{odd } U_n^l(\rho, \theta) &= R_n^l(\rho) \sin(l\theta), \end{aligned} \quad (10)$$

and the radial function $R_n^l(\rho)$ is given by

$$R_n^{n-2m}(\rho) = \sum_{s=0}^m \frac{(-1)^s (n-s)!}{s! (m-s)! (n-m-s)!} \rho^{n-2s}, \quad (11)$$



(a)



(b)

Fig. 4. Normalized Zernike polynomials: (a) U_{21} and (b) U_{22} .

where θ is the angle from the y axis and ρ is the normalized radial distance from the origin. Any circular surface profile can then be expressed as a linear combination of Zernike polynomials:

$$\begin{aligned} W(\rho, \theta) &= \sum_{n=0}^k \sum_{m=0}^n Z_{nm} R_n^{n-2m} \\ &\times \begin{cases} \sin(n-2m)\theta, & \text{if } n-2m > 0 \\ \cos(n-2m)\theta, & \text{if } n-2m \leq 0 \end{cases} \end{aligned} \quad (12)$$

where Z_{nm} are the Zernike coefficients, the weighting terms for each polynomial.

Two polynomials of interest, U_{21} and U_{22} , depicted in Fig. 4, are given by

$$U_{21}(\rho) = 2\rho^2 - 1,$$

$$U_{22}(\rho, \theta) = \rho^2 \cos(2\theta). \quad (13)$$

For small deformations, their respective first-order radii of curvature (R_{21} and R_{22}) can be derived from geometry, yielding

$$\frac{1}{R_{21}} = \frac{4}{R_c^2} Z_{21},$$

$$\frac{1}{R_{22}(\theta)} = \frac{2}{R_c^2} Z_{22} \cos 2\theta, \quad (14)$$

where R_c is the radius of the wafer and Z_{21} and Z_{22} are the Zernike coefficients for U_{21} and U_{22} , respectively. For deformation in the (100) plane, we equate Eqs. (14) and (5) to find

$$Z_{21,(100)} = \frac{3\sigma_o t R_c^2}{2h^2} (s_{11} + s_{12}). \quad (15)$$

For deformation in the (110) plane, we sum the curvatures given by Eqs. (14) and equate it with Eq. (9). From this expression, the Z_{21} and Z_{22} can be related to the isotropic and anisotropic terms, respectively. The Zernike coefficients can then be defined as

$$Z_{21,(110)} = \frac{3\sigma_o t R_c^2}{2h^2} \left(s_{11} + s_{12} - \frac{s}{4} \right),$$

$$Z_{22,(110)} = -\frac{3\sigma_o t R_c^2}{4h^2} S. \quad (16)$$

Equations (15) and (16) express the Zernike coefficients Z_{21} and Z_{22} as functions of the film stress, geometry, and material constants. The out-of-plane deformations for (100) and (110) planes can then be described as linear combinations of isotropic and anisotropic deformations, using Eq. (12), yielding

$$\delta_{(110)}(\rho) = \frac{3\sigma_o t R_c^2}{2h^2} (s_{11} + s_{12})(2\rho^2 - 1),$$

$$\delta_{(110)}(\rho, \theta) = \frac{3\sigma_o t R_c^2}{2h^2} \left(s_{11} + s_{12} - \frac{S}{4} \right) (2\rho^2 - 1) - \frac{3\sigma_o t R_c^2}{4h^2} S(\rho^2 \cos 2\theta). \quad (17)$$

From this Zernike polynomial description, total out-of-plane deformations can be broken down into isotropic and anisotropic terms orthogonal to each other. For (100) planes the deformation is characterized by Z_{21} alone, whereas for (110) planes it is described by both Z_{21} and Z_{22} . The negative sign of the anisotropic term exists because the angular reference is set to the $\langle 110 \rangle$ direction, and can be canceled if the reference frame is rotated by 90° .

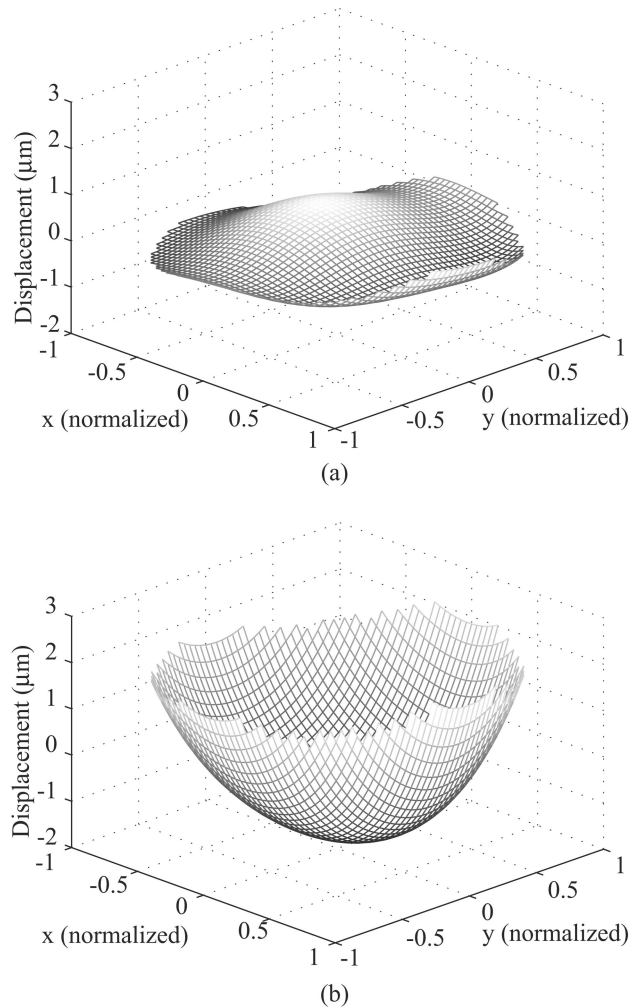


Fig. 5. Measured back wafer surface profile of a (100) silicon wafer (a) before and (b) after deposition of a 20 nm thick Cr film.

4. Experimental Results and Discussion

To test the validity of describing isotropic and anisotropic out-of-plane deformations using Zernike polynomials, an in-house-made Shack–Hartmann (SH) wavefront metrology tool is used.¹² Our SH is an optical setup where collimated deep-UV ($\lambda \sim 254$ nm) light is reflected off the tested wafer surface onto wavefront sensors. The wavefront is focused by a microlenslet array to individual focal spots, which are captured by a CCD camera. By comparing the relative displacements of the spots with those from an optical reference flat, a local slope field can be calculated and used to reconstruct the wafer surface using a least-squares fit algorithm to the Zernike polynomials.¹³ By mapping the back surface of the wafer before and after depositing the thin film, the out-of-plane deformation can be characterized.

Silicon wafers 100 mm in diameter, 0.5 mm thick, and (100) and (110) orientations were used in the experiment. Both type of wafers have their primary flat along the $\langle 100 \rangle$ direction. We deposited 20 nm of Cr by *e*-beam evaporation on the front, and the back surfaces were measured before and after deposition.

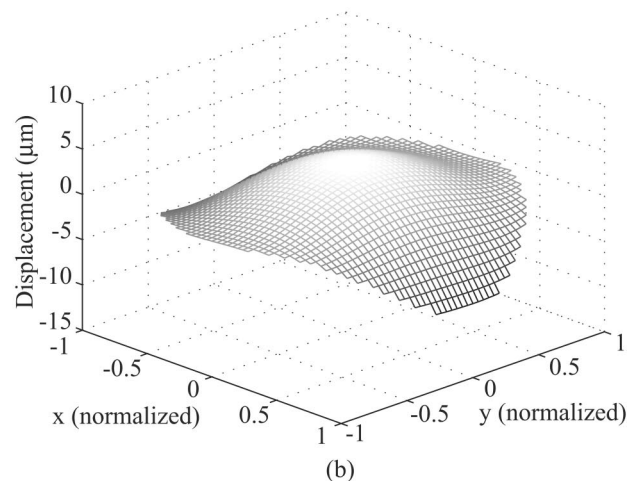
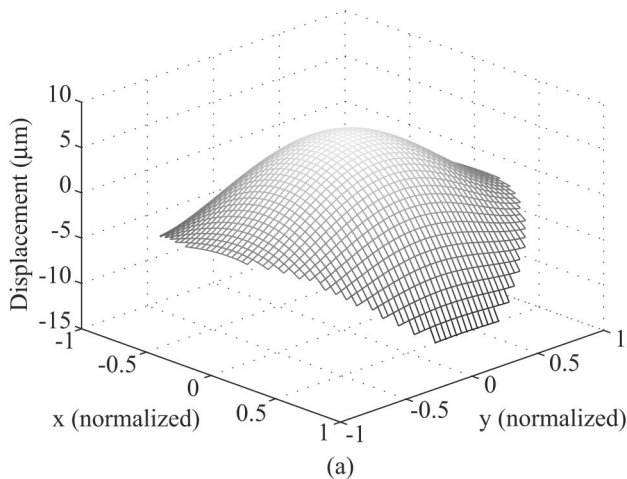


Fig. 6. Measured back wafer surface profile of a (110) silicon wafer (a) before and (b) after deposition of a 20 nm thick Cr film.

During measurements the wafer was held by a thin foil optic constraint¹⁴ with the primary flat downward, as depicted in Fig. 2. The thin optic metrology truss, having a dynamic repeatability of ~ 40 nm and inducing extremely low distortion, is critical in the measurements.

The experimentally measured (100) and (110) wafer back surfaces, before and after the film deposition, are illustrated in Figs. 5 and 6. The distortion caused by the thin-film residual stress is evident; yet, because of the initial wafer nonflatness, the deformations are difficult to analyze. The wafer surfaces are fitted to the first four orders of the Zernike polynomials, and their associated Zernike coefficients are tabulated in Table 1. Higher-order polynomials are not significant, since wafer nonflatness typically does not include variations with higher spatial frequencies.

As the experimental results show, for (100) silicon there is only significant change in the Z_{21} coefficient, having changed by $2.05 \mu\text{m}$, whereas for (110) silicon there are significant changes in the Z_{21} and Z_{22} , having changed by 2.64 and $-0.97 \mu\text{m}$, respectively. The changes in the other coefficients are all relatively

Table 1. Zernike Coefficients for Measured Back Wafer Surface Profiles of (100) and (110) Silicon before and after the Deposition of a 20 nm Thick Cr Film

Zernike Coefficient (μm)	(100) Si			(110) Si		
	Before	After	Change	Before	After	Change
Z_{20}	0.090	0.035	-0.055	0.571	0.508	-0.063
Z_{21}	-0.287	1.759	2.046	-5.946	-3.308	2.639
Z_{22}	0.114	0.116	0.002	3.587	2.619	-0.968
Z_{30}	0.113	0.088	-0.025	-0.596	-0.657	-0.062
Z_{31}	-0.408	-0.309	0.099	0.832	0.893	0.061
Z_{32}	-0.045	-0.019	0.027	0.223	0.245	0.023
Z_{33}	0.110	0.093	-0.017	0.338	-0.286	0.052
Z_{40}	0.025	0.014	-0.012	-0.147	-0.161	-0.015
Z_{41}	-0.015	-0.027	-0.012	-0.204	-0.216	-0.013
Z_{42}	0.276	0.269	-0.007	0.721	0.699	-0.022
Z_{43}	-0.079	-0.080	-0.002	0.585	0.563	-0.022
Z_{44}	0.196	0.187	-0.009	-0.986	-0.978	0.008

small, and are comparable to the repeatability of the measurement system. From these data it is obvious that there is one dominant mode of distortion for (100) silicon and two modes for (110) silicon, Z_{21} describing the isotropic and Z_{22} the anisotropic terms. For linear elastic deformation, the equations derived previously are valid in terms of ΔZ_{21} and ΔZ_{22} . Assuming no deformation at the center of the wafer, the out-of-plane deformation across the entire wafer is then

$$\delta_{(110)}(\rho) = 4.09\rho^2 \mu\text{m},$$

$$\delta_{(110)}(\rho, \theta) = 5.28\rho^2 - 0.97\rho^2 \cos 2\theta \mu\text{m}. \quad (18)$$

For the more interesting case of (110) silicon, the experimental results can be compared with the analytical model derived earlier. The theoretical ratio of the anisotropic to the isotropic curvature terms in Eq. (9) is dependent on the compliances of the materials. For silicon it is given by

$$-\frac{S}{4(s_{11} + s_{12}) - S} = -0.189. \quad (19)$$

This ratio can be compared with the measured ratio of the isotropic and anisotropic Zernike coefficients,

$$\frac{\Delta Z_{22}}{2\Delta Z_{21}} = -0.183 \pm 0.004, \quad (20)$$

where all errors reported here are estimated from the 1σ repeatability of the measurement system. The close agreement between theory and experimental results (error $\sim 3\%$) demonstrates the validity of the model.

From the measured ΔZ_{21} , the film stress on the (100) silicon can be obtained, yielding

$$\sigma_{21, (100)} = \frac{2h^2}{3tR_c^2} \frac{\Delta Z_{21}}{(s_{11} + s_{12})} = 2.32 \pm 0.02 \text{ GPa.} \quad (21)$$

For (110) silicon, the stress can be calculated from both the isotropic and the anisotropic terms, obtaining

$$\sigma_{21, (110)} = \frac{2h^2}{3tR_c^2} \frac{\Delta Z_{21}}{\left(s_{11} + s_{12} - \frac{S}{4}\right)} = 3.56 \pm 0.03 \text{ GPa,}$$

$$\sigma_{22, (110)} = -\frac{4h^2}{3tR_c^2} \frac{\Delta Z_{22}}{S} = 3.47 \pm 0.07 \text{ GPa,} \quad (22)$$

which agree within $\sim 3\%$. Since the back surface profile was measured for the experiments, the sign of the stress needs to be reversed, yielding a compressive stress in the film. The small errors are believed to be caused by the repeatability of the optical setup, limited by various factors such as air turbulence, temperature gradient, and unstable light source.

5. Conclusion

The isotropic and anisotropic out-of-plane deformations of (100) and (110) planes for cubic materials induced by thin-film residual stress are studied and described using Zernike polynomials. Combining the derived modified Stoney's equation with the Zernike polynomial description, the deformation can be decomposed into isotropic and anisotropic terms. Experimental results by use of (100) and (110) silicon wafers show that there are changes only in the Z_{21} and Z_{22} coefficients, corresponding to isotropic and anisotropic deformations. For (110) silicon, the measured ratio of anisotropic to isotropic terms agrees with the analytical model to within $\sim 3\%$.

We gratefully acknowledge the outstanding technical assistance of Robert Fleming, Jim Carter, and Jim Daley. Student, staff, and facility support from the Space Nanotechnology Laboratory, NanoStructures Laboratory, and Microsystems Technology Laboratory at MIT are also appreciated. This work

was supported by NASA grants NAG5-12583 and NAG5-5405.

References

1. L. B. Freund and S. Suresh, *Thin Film Materials: Stress, Defect Formation and Surface Evolution* (Cambridge U. Press, 2003).
2. M. Madou, *Fundamentals of Microfabrication* (CRC Press, 1997).
3. A. E. Franke, M. L. Schattenburg, E. M. Gullikson, J. Cottam, S. M. Kahn, and A. Rasmussen, "Supersmooth x-ray reflection grating fabrication," *J. Vac. Sci. Technol. B* **15**, 2940–2945 (1997).
4. C.-H. Chang, J. C. Montoya, M. Akilian, A. Lapsa, R. K. Heilmann, M. L. Schattenburg, M. Li, K. A. Flanagan, A. P. Rasmussen, J. F. Seely, J. M. Laming, B. Kjornrattanawanich, and L. I. Goray, "High fidelity blazed grating replication using nanoprint lithography," *J. Vac. Sci. Technol. B* **22**, 3260–3264 (2004).
5. G. G. Stoney, "The transition of metallic films deposited by electrolysis," *Proc. R. Soc. London Ser. A* **82**, 172–175 (1909).
6. W. A. Brantley, "Calculated elastic constants for stress problems associated with semiconductor devices," *J. Appl. Phys.* **44**, 534–535 (1973).
7. A. J. Schell-Sorokin and R. M. Tromp, "Mechanical stresses in (sub)monolayer epitaxial films," *Phys. Rev. Lett.* **64**, 1039–1042 (1990).
8. D. Sander, A. Enders, and J. Kirschner, "A simple technique to measure stress in ultrathin films," *Rev. Sci. Instrum.* **66**, 4734–4735 (1995).
9. P. M. Marcus, "Epitaxial strain and epitaxial bending," *Surf. Sci.* **366**, 219–227 (1996).
10. W. P. Mason, *Physical Acoustics and the Properties of Solids* (Van Nostrand, 1958).
11. D. Malacara, *Optical Shop Testing* (Wiley, 1992).
12. C. R. Forest, C. R. Canizares, D. R. Neal, M. McGuirk, and M. L. Schattenburg, "Metrology of thin transparent optics using Shack-Hartmann wavefront sensing," *Opt. Eng.* **43**, 742–753 (2004).
13. D. R. Neal, W. J. Alford, J. K. Gruetzner, and M. E. Warren, "Amplitude and phase beam characterization using a two-dimensional wavefront sensor," in *Third International Workshop on Laser Beam and Optics Characterization*, M. Morin and A. Giesen, eds., *Proc. SPIE* **2870**, 72–82 (1996).
14. M. Akilian, C. R. Forest, A. H. Slocum, D. L. Trumper, and M. L. Schattenburg, "Thin optical constraint," in *Proceedings of the 19th Annual Meeting of the American Society for Precision Engineering* (ASPE, 2004), Vol. 34, pp. 209–212.